ADVANCES IN ATMOSPHERIC SCIENCES, VOL. 36, MARCH 2019, 292–302

• **Original Paper** •

Verification and Improvement of the Ability of CFSv2 to Predict the Antarctic Oscillation in Boreal Spring

Dapeng ZHANG[1,2], Yanyan HUANG*[1,2], Bo SUN[1,2], Fei LI[1,2,3], and Huijun WANG[1,2]

[1]*Collaborative Innovation Center on Forecast and Evaluation of Meteorological Disasters/Key Laboratory of Meteorological Disaster, Ministry of Education, Nanjing University of Information Science and Technology, Nanjing* 210044*, China*

[2]*Nansen–Zhu International Research Centre, Institute of Atmospheric Physics, Chinese Academy of Sciences, Beijing* 100029*, China*

[3]*NILU – Norwegian Institute for Air Research, Kjeller* 2007*, Norway*

(Received 6 May 2018; revised 14 October 2018; accepted 29 October 2018)

ABSTRACT

The boreal spring Antarctic Oscillation (AAO) has a significant impact on the spring and summer climate in China. This study evaluates the capability of the NCEP's Climate Forecast System, version 2 (CFSv2), in predicting the boreal spring AAO for the period 1983–2015. The results indicate that CFSv2 has poor skill in predicting the spring AAO, failing to predict the zonally symmetric spatial pattern of the AAO, with an insignificant correlation of 0.02 between the predicted and observed AAO Index (AAOI). Considering the interannual increment approach can amplify the prediction signals, we firstly establish a dynamical–statistical model to improve the interannual increment of the AAOI (DY_AAOI), with two predictors of CFSv2-forecasted concurrent spring sea surface temperatures and observed preceding autumn sea ice. This dynamical–statistical model demonstrates good capability in predicting DY_AAOI, with a significant correlation coefficient of 0.58 between the observation and prediction during 1983–2015 in the two-year-out cross-validation. Then, we obtain an improved AAOI by adding the improved DY_AAOI to the preceding observed AAOI. The improved AAOI shows a significant correlation coefficient of 0.45 with the observed AAOI during 1983–2015. Moreover, the unrealistic atmospheric response to March–April–May sea ice in CFSv2 may be the possible cause for the failure of CFSv2 to predict the AAO. This study gives new clues regarding AAO prediction and short-term climate prediction.

Key words: Antarctic Oscillation, interannual-increment approach, CFSv2, dynamical–statistical model, prediction

Citation: Zhang, D. P., Y. Y. Huang, B. Sun, F. Li, and H. J. Wang, 2019: Verification and improvement of the ability of CFSv2 to predict the Antarctic Oscillation in boreal spring. *Adv. Atmos. Sci.*, **36**(3), 292–302, https://doi.org/10.1007/s00376-018-8106-6.

1. Introduction

The Antarctic Oscillation (AAO), which is also called the Southern Annular Mode, is a leading mode of the variability of extratropical atmospheric circulation in the Southern Hemisphere (SH) (Gong and Wang, 1998, 1999). The AAO is characterized by opposite anomalies between the mid- and high-latitude regions of the SH in sea level pressure (SLP), as well as in geopotential height, air temperature, and zonal wind. The positive phase of the AAO refers to positive (negative) anomalies of SLP in the mid (high) latitudes, and vice versa (Gong and Wang, 1998; Fyfe et al., 1999; Fan and Wang, 2006; Screen et al., 2010). This zonally symmetric pattern of the AAO possesses a barotropic structure, which can be observed through the troposphere and the lower stratosphere (Thompson and Solomon, 2002). Essentially, the AAO involves an exchange of mass and energy between the mid and high latitudes of the SH (Thompson and Wallace, 2000; Fan and Liu, 2013).

The AAO dominates the seasonal, interannual, and interdecadal variability of SH climate, exerting important impacts on the rainfall over Australia and South America and surface air temperatures over the Antarctic region (Silvestri and Vera, 2003; Lovenduski and Gruber, 2005; Hendon et al., 2007; Marshall and Bracegirdle, 2015). The AAO also influences the frequency of Atlantic tropical hurricanes and the North American summer monsoon (Fan, 2009a; Sun, 2010). Moreover, it has been suggested that the boreal spring AAO can notably influence the East Asian climate, especially the summer climate, via several teleconnection effects (Gao et al., 2003; Xue et al., 2003; Fan and Wang, 2004; Sun et al., 2009). Specifically, Xue et al. (2003) indicated that a positive-phase boreal spring AAO induces a strengthened Masklin high and Australian high, which further induces increased summer rainfall in the Yangtze River valley region in China

* Corresponding author: Yanyan HUANG
Email: huangyy@nuist.edu.cn

and Japan. Fan and Wang (2004) suggested that the interannual variation of the boreal winter and spring AAO has an effect on the frequency of dust weather in North China during spring though modulating a meridional wave train across the southern and northern hemispheres. In addition, Sun et al. (2009) found that a positive-phase boreal spring AAO is also concurrent with strengthened convective activity over the Maritime Continent, which influences the western Pacific subtropical high and results in an increase in summer rainfall over the Yangtze River valley region of China. Considering the importance of the boreal spring AAO to the variability of the SH climate and boreal summer climate over East Asia, it is important to obtain skillful predictions of the spring AAO by means of dynamical and statistical models.

The NCEP's Climate Forecast System, version 2 (CFSv2), has been documented as a useful tool for seasonal forecasting (Pokhrel et al., 2012; Jiang et al., 2013; Riddle et al., 2013; Tian et al., 2018). Many aspects of CFSv2's forecast models and data assimilation systems represent improvements over its previous version (CFSv1), and it possesses good skill in making subseasonal and/or seasonal predications of the Madden–Julian Oscillation, surface temperatures over North America, and global sea surface temperatures (SSTs) (Kumar et al., 2012; Saha et al., 2014). However, few studies have evaluated the skill of CFSv2 in predicting the seasonal AAO, especially the boreal spring AAO.

Using the interannual-increment approach, Fan et al. (2008) constructed a physical-based statistical model for predicting the summer rainfall in the middle–lower Yangtze River valley region, the results of which demonstrated the model has good skill and an advantage of the interannual-increment approach. Instead of using original variables, the interannual-increment approach uses the year-to-year increment/decrement (DY, the difference in a variable between the current and preceding year) of variables as the predictor and/or predictand. Considering the quasi-biennial oscillation of the variability of the tropospheric climate, the main advantage of the interannual-increment approach is that the year-to-year increment/decrement amplifies the signals of interannual variability of the predictors and/or predictand, whereby a more efficient physical–empirical model can be established (Fan et al., 2008; Sun and Wang, 2013; Huang et al., 2014). Specifically, if Y_i and Y_{i-1} represent the variable in the current and previous year, respectively, then $Y_i = C + P_i$ and $Y_{i-1} = -C + P_{i-1}$ in which P_i and P_{i-1} represent a disturbance in C. After ignoring the disturbance, the climatological mean is $a \approx 0$, the anomaly of Y is $Y_i' = Y_i - a \approx C$, and the year-to-year increment is $\mathrm{DY}_i = Y_i - Y_{i-1} \approx 2C$, suggesting that the amplitude of a variable in the form of the year-to-year increment is twice the value of the anomaly (Wang et al., 2010; Huang et al., 2014). To date, the interannual-increment approach has been utilized in a series of studies for predicting the summer rainfall over the Yangtze River valley region (Fan et al., 2008), temperatures over northeastern China (Fan, 2009b), the frequency of tropical cyclones landing in China (Fan, 2009c), the North Atlantic Oscillation (Tian and Fan, 2015; Fan et al., 2016), the summer Asian–Pacific Oscillation (Huang et al., 2014), and winter haze days (Yin and Wang, 2016), among others. However, the capability of this interannual-increment approach for predicting the AAO has not yet been examined.

In this study, the skill of CFSv2 in predicting the boreal spring AAO is evaluated, and a dynamical–statistical model is established to improve the CFSv2-forecasted boreal spring AAO based on the interannual-increment approach, utilizing CFSv2-forecasted concurrent boreal spring SSTs and observed preceding boreal autumn sea ice as two predictors. The data and methods are described in section 2. Section 3 evaluates the prediction skill of the AAO in CFSv2. In section 4, the dynamical–statistical model is established and used to improve the prediction of the AAO. Section 5 discusses the reasons for the failure of CFSv2 to predict the AAO. Conclusions are drawn in section 6.

2. Data and methods

2.1. *Data*

The monthly hindcasts ($1^\circ \times 1^\circ$) of SLP, SST and sea-ice concentration (SIC) used in this study for March–April–May (MAM) during 1982–2015 are derived from CFSv2, which is operated with a fully coupled atmosphere–ocean–sea-ice–land model (Saha et al., 2014). The CFSv2 hindcasts are performed (0000, 0600, 1200 and 1800 UTC) for nine months, with initial conditions every five days, from 11 January to 5 February, in the MAM SLP, SST and SIC hindcast. The monthly data of the ensemble mean of these 24 forecasts is used in this study (http://nomads.ncdc.noaa.gov/data/cfsr-rfl-mmts/).

The observational data used in this study include monthly SLP ($2.5^\circ \times 2.5^\circ$) derived from NCEP-1 (Kalnay et al., 1996), SST ($2^\circ \times 2^\circ$) from ERSST.v3b (Smith et al., 2008), and SIC ($1^\circ \times 1^\circ$) from the Met Office Hadley Center (https://www.metoffice.gov.uk/hadobs/hadisst/) (Rayner et al., 2003). All datasets are interpolated to a $2.5^\circ \times 2.5^\circ$ horizontal resolution using bilinear interpolation. Considering that this study focuses on interannual variability, all the data during 1983–2015 are detrended.

The Antarctic Oscillation Index (AAOI) of boreal spring used in this study is defined as the time series of the leading empirical orthogonal function (EOF) mode of boreal spring SLP anomalies south of 20°S (Fan and Wang, 2006).

2.2. *Methods*

A dynamical–statistical model is established to improve the CFSv2-forecasted AAOI, based on the original numerical forecast of CFSv2 and a physical–statistical approach. The relationship of the boreal spring AAOI with concurrent SSTs and preceding autumn SIC is analyzed, whereby the physical–statistical approach utilizes the CFSv2-forecasted boreal spring SSTs and observed preceding autumn SIC as two predictors of the boreal spring AAOI, using a linear regression method. The dynamical–statistical model is expected to take into account information that might be misrep-

resented in CFSv2 regarding the dynamical processes linking preceding autumn SIC with the boreal spring AAO. Accordingly, an improved prediction of the AAOI is expected based on this dynamical–statistical model.

The dynamical–statistical model is validated using the methods of two-years-out cross-validation (Michaelsen, 1987; Blockeel and Struyf, 2003), correlation, and root-mean-square error (RMSE) for the period 1983–2015. The two-years-out cross-validation method predicts the predictand in the specific two years with a model built by the sample of leaving these two years out. The statistical significance of correlation coefficients is estimated using the Student's *t*-test.

3. Predictive skill of CFSv2

Considering that the AAO mode is defined as the leading EOF mode of SLP, the predictive skill of CFSv2 for MAM mean SLP is firstly evaluated. Figure 1 shows the climatological MAM mean SLP south of 20°S during 1983–2015 for observations and CFSv2. The CFSv2 prediction is consistent with the observation regarding the spatial pattern of MAM mean SLP, which is characterized by relatively high SLPs over the low- and midlatitudes and relatively low SLPs over the Southern Ocean and particularly high SLPs over Antarctica. The corresponding correlation coefficient between the CFSv2 prediction and observation for the spatial pattern of MAM mean SLP has a value of 0.96, significant at the 95% confidence level, indicating a good capability of CFSv2 for predicting SLP. However, the SLPs over the high latitudes are underestimated in the CFSv2 prediction in comparison to observation, where the observed MAM mean SLPs over the high latitudes are mostly above 1040 hPa (Fig. 1a), whereas the CFSv2-predicted MAM mean SLPs are mostly about 1020 hPa over these regions (Fig. 1b). Specifically, the CFSv2-predicted MAM mean SLPs are generally 20 hPa smaller than observed over Antarctica (Fig. 1).

In addition, the CFSv2-predicted MAM SLPs exhibit a limitation in the amplitude of interannual variability, which is measured by the standard deviation of the time series of SLPs for each grid. As shown in Fig. 2, the CFSv2-predicted SLPs show a noticeable underestimation for the interannual variability of MAM SLPs over the SH relative to observed results. The observed interannual variability of MAM SLPs highlights a gradient from small amplitudes of interannual variability in the low latitudes toward large amplitudes of interannual variability in Antarctica (Fig. 2a). By contrast, the CFSv2 prediction does not highlight this gradient, instead highlighting large amplitudes of SLP interannual variability

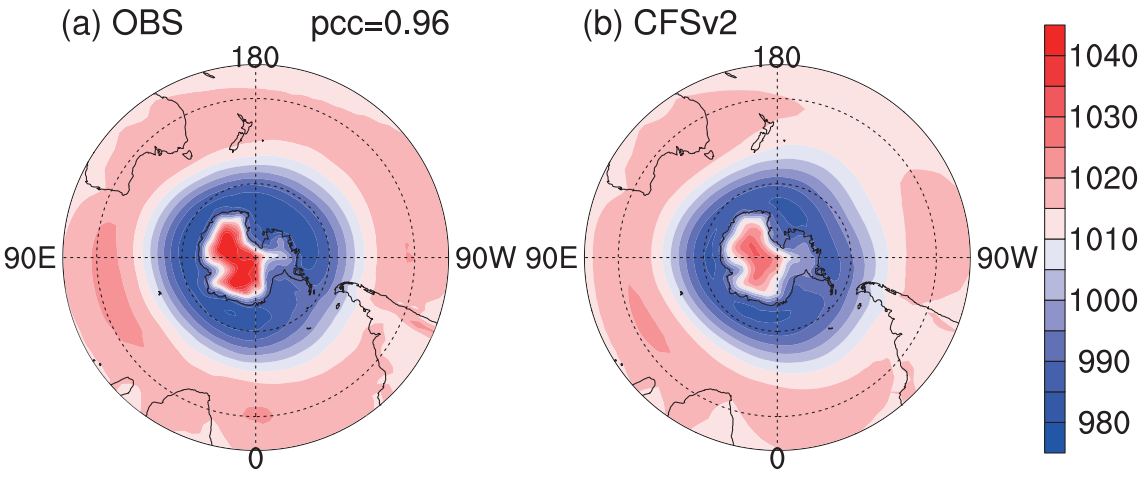

Fig. 1. MAM mean SLP (units: hPa) south of 20°S during 1983–2015 derived from (a) observation and (b) CFSv2.

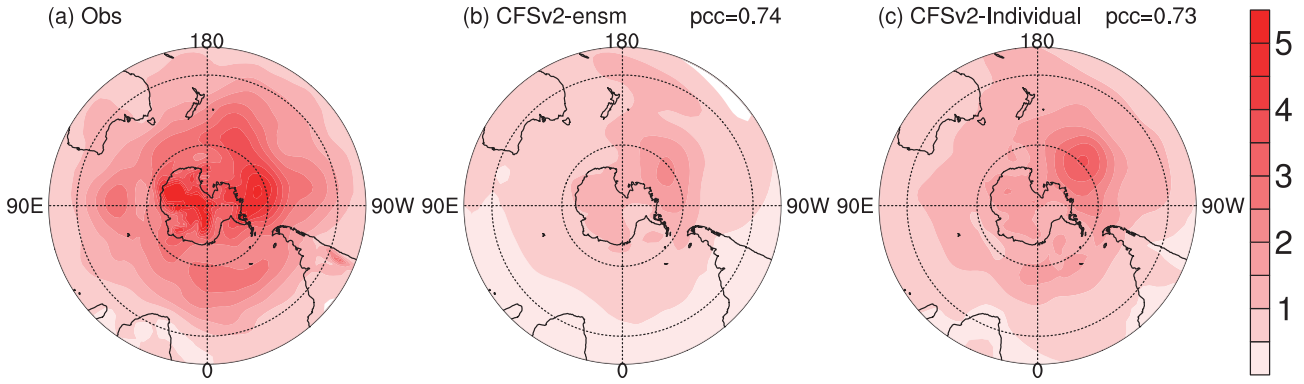

Fig. 2. Standard deviation of MAM mean SLP (units: hPa) south of 20°S during 1983–2015 derived from (a) observation, (b) ensemble data, and (c) individual data from CFSv2.

over the southern Pacific (Fig. 2b). The standard deviation of the CFSv2-predicted SLPs for individual members is also evaluated, showing that most individual members underestimate the standard deviation of MAM SLP (Fig. 2c), which is similar to the ensemble mean results (Fig. 2b). These abovementioned limitations of the CFSv2 prediction act as a disadvantage in achieving a good prediction of the AAO.

Accordingly, Fig. 3 shows the leading EOF modes of MAM SLP anomalies during 1983–2015 south of 20°S for observed and CFSv2-predicted MAM AAO modes. The CFSv2-predicted AAO mode overall represents a contrasting relationship between the subtropical highs and circumpolar lows (Fig. 3b), resembling the observed AAO mode to an extent. Correspondingly, the correlation coefficient between the CFSv2-predicted and observed MAM AAO modes has a value of 0.56, significant at the 95% confidence level. On the other hand, a few notable discrepancies are detected between the observed and CFSv2-predicted MAM AAO modes regarding the positions of anomalous centers. For the observed MAM AAO mode, there are three anomalous positive centers located in the midlatitude Pacific, Atlantic, and Indian oceans (Fig. 3a); whereas, for the CFSv2-predicted MAM AAO mode, large positive anomalies are found over the midlatitude Pacific region, while small positive anomalies are found over the midlatitude Atlantic and Indian oceans (Fig. 3b). Moreover, a significant anomalous low center characterizes the CFSv2-predicted MAM AAO mode in the southern Pacific, which is not detected for the observed MAM AAO mode. These discrepancies disqualify CFSv2 for predicting the zonally symmetric pattern of the MAM AAO mode, notwithstanding the abovementioned significant correlation coefficient. Moreover, the AAO patterns predicted by individual members is assessed, showing that these individual members possess poorer skill in predicting the zonally symmetric pattern of the AAO mode (not shown) than the ensemble mean result (Fig. 3b).

The corresponding time series derived from observation and CFSv2 (i.e., the AAOI) during 1983–2015 show an insignificant correlation, with a correlation coefficient of 0.02, indicating a bad performance of CFSv2 in predicting the interannual variation of the MAM AAO (Fig. 4). The time series (AAOIs) are both projections of the observed AAO mode (Fig. 3a). As shown in Fig. 4a, the CFSv2-predicted AAOI is essentially inconsistent with the observed AAOI, failing in representing the significant positive (negative) AAOI values in 1989, 1998, 1999 and 2006 (1990, 1992 and 2002) and dramatically misrepresenting the signs of the AAOI values for the early 1990s, late 1990s and early 2000s. The corresponding DY_AAOI also indicates an inconsistency between the observed results and CFSv2-predicted results, which exhibit an opposing relationship for a number of years, such as 1983, 1990, 1992, 1993, 1998, 2001 and 2004, with a low correlation coefficient of 0.03 (Fig. 4b). Thus, the CFSv2 prediction for the MAM AAO is far from good enough, which demands improvements.

4. Improvements of the prediction of the AAO

Wavelet analysis of the MAM AAOI during 1983–2015 indicates that the AAO has a two-year period (Fig. 5), indicating it is reasonable to use the interannual increment approach to improve the AAO prediction. A dynamical–statistical model is established to improve the prediction of MAM DY_AAOI in this section. Then, an improved AAOI is obtained by adding the improved DY_AAOI prediction to the observed MAM AAOI for the previous year. The predictors utilized in this model, the approach of this dynamical–statistical model, and the validation of the results, are discussed as follows.

4.1. *Predictors*

The predictors for the MAM AAO can be selected via two ways. One way is to select the predictor/s that has/have a lead–lag relationship with the MAM AAO, which can be

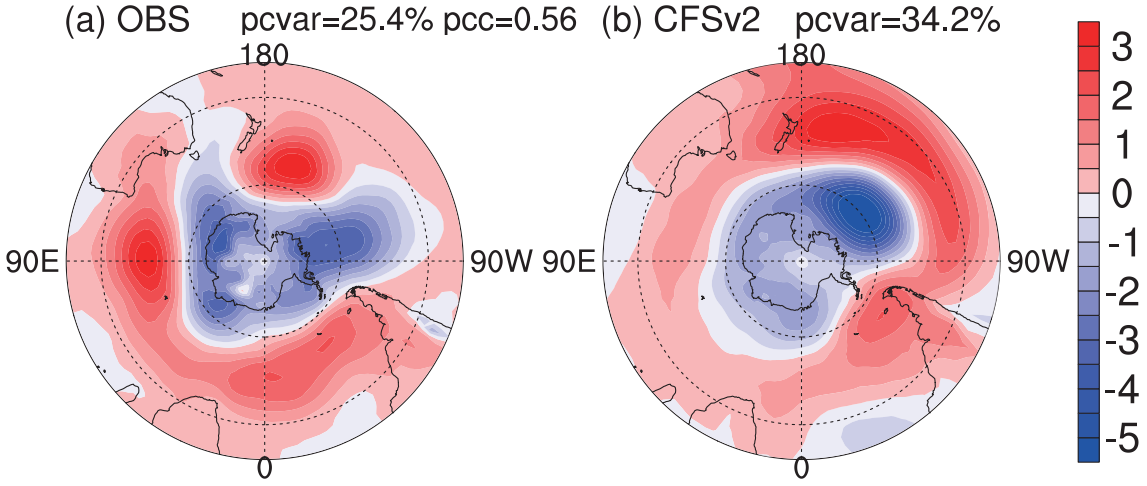

Fig. 3. Spatial patterns of the leading EOF mode of MAM SLP anomalies (units: hPa) south of 20°S during 1983–2015 derived from (a) observation and (b) CFSv2. The abbreviations pcvar and pcc represent the percentage variance and spatial correlation coefficient of the leading EOF modes between observation and CFSv2, respectively.

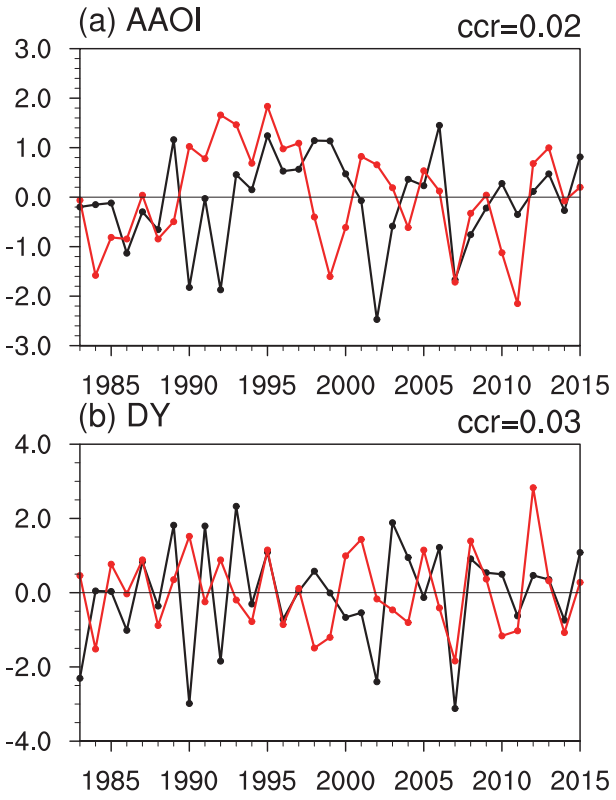

Fig. 4. The normalized (a) MAM AAOI and (b) DY_AAOI during 1983–2015 derived from observation (black line) and CFSv2 (red line). The corresponding correlation coefficient between the two time series is labeled in the top-right corner.

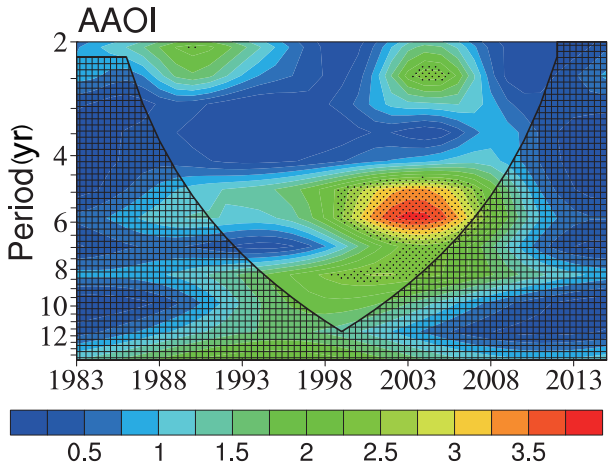

Fig. 5. Wavelet analysis of the MAM AAOI for the period 1983–2015. Dotted regions indicate significant variability at the 90% confidence level estimated by a red noise process, and the parabola indicates the "cone of influence".

derived from the observational data for the months preceding MAM. The other way is to select factor/s concurrent with the MAM AAO that is/are well predicted by CFSv2, such as SST. It has been suggested that the seasonal predictability of the climate largely depends on the interaction between the ocean and atmosphere (Kushnir et al., 2002). Accordingly, two predictors that have considerable effects on the MAM AAO are selected for the dynamical–statistical model: the preceding SON SIC and concurrent MAM SSTs in the SH, which are derived from the observational data and CFSv2 predictions, respectively.

The SIC can influence the atmosphere by changing the surface radiation balance and heat exchange because of its albedo effect (Stammerjohn and Smith, 1997; Zhang, 2007; Stammerjohn et al., 2008; Raphael et al., 2011; Xu et al., 2018). A significant lead–lag correlation relationship between the Antarctic SIC and MAM AAO was found by Gao et al. (2003), where the Antarctic SIC leads the MAM AAO for two and six months, especially for the six-month lead–lag relationship. It has also been suggested that the Antarctic dipole–like sea-ice anomalies in boreal late autumn and winter have an important impact on the MAM AAO (Wu and Zhang, 2011). The Antarctic dipole–like SIC pattern is characterized by an out-of-phase relationship between SIC anomalies in the Weddell Sea and SIC anomalies in the Bellinsgauzen–Amundsen Sea. Positive SIC anomalies in the Weddell Sea and negative SIC anomalies in the Bellinsgauzen–Amundsen Sea in boreal autumn can cause anomalous poleward (equatorward) transient eddy momentum fluxes in the high (mid) latitudes of the SH, the effects of which persist through the following boreal spring and result in a poleward displacement of the tropospheric westerlies associated with the MAM AAO (Limpasuvan and Hartmann, 2000; Deser et al., 2007; Wu and Zhang, 2011). Thus, the preceding SON SIC in the Weddell Sea and Bellinsgauzen–Amundsen Sea can be considered a predictor for the dynamical–statistical model.

Figure 6a shows the distribution of the correlation coefficients between the preceding SON SIC and MAM AAOI during 1983–2015. A large area of significant positive correlation is found in the Weddell Sea and a relatively small area of negative correlation is found in the Bellinsgauzen–Amundsen Sea, indicating an influence of the preceding SON Antarctic dipole on the MAM AAO. In addition, the correlation coefficients between the corresponding DY_SIC and DY_AAOI are computed. As shown in Fig. 6b, the DY_SIC and DY_AAOI exhibit a more significant correlation in the Bellinsgauzen–Amundsen Sea than the abovementioned correlation between the SIC and AAOI. The positive correlation coefficients between DY_SIC and DY_AAOI in the Weddell Sea are also of more significance than those between the SIC and AAOI. This increased correlation between DY_SIC and DY_AAOI reflects the advantage of the interannual-increment approach for amplifying the signals of interannual variability. Hence, the area-weighted areal mean SON DY_SICs in two key regions are calculated to be the sea-ice indices (DY_SICI), with Region-1 covering (60°–71°S, 30°–60°W) for positive correlation coefficients between DY_SIC and DY_AAOI and Region-2 covering (67°–73°S, 77°–108°W) for negative correlation coefficients, as shown in Fig. 6b. Hereinafter, the DY_SICI for Region-1 is labeled as DY_SICI_R_1, and the DY_SICI for Region-2 is labeled as DY_SICI_R_2. For com-

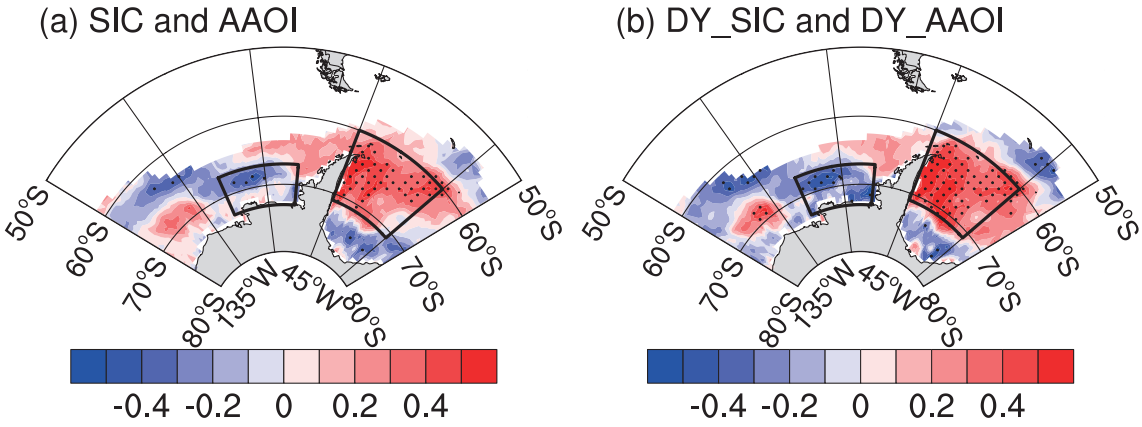

Fig. 6. (a) Correlation coefficients between the preceding SON SIC and MAM AAOI derived from observation during 1982/83–2014/15. (b) As in (a), but for the DY of sea ice and the DY of AAOI. Dotted areas indicate statistical significance at the 95% confidence level, based on the Student's *t*-test. The black curvilinear rectangles represent the key regions of SON SIC influencing MAM AAO.

parison, the area-weighted areal mean SON SICs for Region-1 and Region-2 are also computed and labeled as SICI_R_1 and SICI_R_2, respectively. The correlation coefficient between DY_AAOI and DY_SIC_R_1 (DY_SIC_R_2) is 0.48 (−0.38), which is at the 99% (95%) confidence level. The correlation coefficient between AAOI and SIC_R_1 (SIC_R_2) is 0.43 (−0.24), which is at (below) the 95% confidence level. Thus, DY_SIC_R_1 and DY_SIC_R_2 are used in the dynamical–statistical model for predicting DY_AAOI.

The variability of the SH atmosphere is significantly influenced by tropical and SH SSTs (Zhou and Yu, 2004; Gupta and England, 2007; Li et al., 2015). It is found that the tropical SSTs may influence the AAO via affecting the intensity and latitudinal displacement of the Hadley circulation. Specifically, positive SST anomalies in the tropical central Pacific can cause a strengthened Hadley cell and a poleward-shifted SH subtropical jet, which further causes an anomalous convergence of eddy momentum flux in the midlatitudes and a equatorward shift of the eddy-driven jet; consequently, the westerlies and eddy momentum flux convergence are weakened in the high latitudes on the poleward side of the eddy-driven jet, contributing to a negative-phase MAM AAO, and vice versa (Seager et al., 2003; Lim et al., 2013; Han et al., 2017). In addition, the extratropical SSTs also have a significant, albeit weak, influence on the atmosphere. During boreal winter and spring, positive SST anomalies in the midlatitude South Pacific and negative SST anomalies in the high-latitude Southern Ocean cause a strengthened Ferrel cell and a strengthened circumpolar low in the SH, resulting in a positive-phase AAO (Mo, 2000; Fan and Wang, 2007; Hao et al., 2017). Considering the significant impact of concurrent SST on the MAM AAO and the good skill of CFSv2 in predicting SST (Saha et al., 2014), the CFSv2-predicted MAM SST may be used as another predictor for the dynamical–statistical model.

Figure 7 shows the correlation coefficients between the observed MAM AAOI (DY_AAOI) and concurrent CFSv2-predicted SST (DY_SST) during 1983–2015. The observed MAM AAOI and CFSv2-predicted SST exhibit a negative correlation in the tropical central Pacific and a positive correlation to the east of Australia (Fig. 7a). Nevertheless, for most areas of the SH Pacific, the SSTs have an insignificant correlation with the MAM AAOI (Fig. 7a). On the other hand, the observed MAM DY_AAOI and CFSv2-predicted DY_SST exhibit a more significant relationship in the midlatitude South Pacific, with significant correlation coefficients in the central South Pacific and to the east of Australia (Fig. 7b). In particular, considering that the interannual-increment approach can largely increase the signal of the predictand, the positive correlation coefficients in the midlatitude southeastern Pacific occupy a large area that is not observed for the correlation coefficients between the MAM AAOI and CFSv2-predicted SSTs, which reflects a significant relationship between the MAM AAOI and concurrent SSTs revealed by the interannual-increment approach.

Hence, the area-weighted areal mean MAM DY_SSTs of the CFSv2 prediction in two key regions are calculated to be SST indices (DY_SSTI): Region-3 covering the midlatitude southeastern Pacific (19°–37°S, 100°–135°W) for positive correlation coefficients, and Region-4 covering the equatorial central Pacific (5°N–4°S, 175°E–145°W) for negative correlation coefficients between DY_SST and DY_AAOI, as shown in Fig. 7b. Hereinafter, the DY_SSTI for Region-3 is labeled as DY_SSTI_R_3, and the DY_SSTI for Region-4 is labeled as DY_SSTI_R_4. For comparison, the area-weighted areal mean MAM SST of the CFSv2 prediction for Region-3 and Region-4 are also computed and labeled as SSTI_R_3 and SSTI_R_4, respectively. The correlation coefficient between DY_AAOI and DY_SSTI_R_3 (DY_SSTI_R_4) is 0.49 (−0.37), which is at the 99% (95%) confidence level. The correlation coefficient between AAOI and SSTI_R_3 (SSTI_R_4) is 0.05 (−0.33), which is below (at) the 95% confidence level. In particular, a significant correlation is found between the time series of the CFSv2-predicted and observed

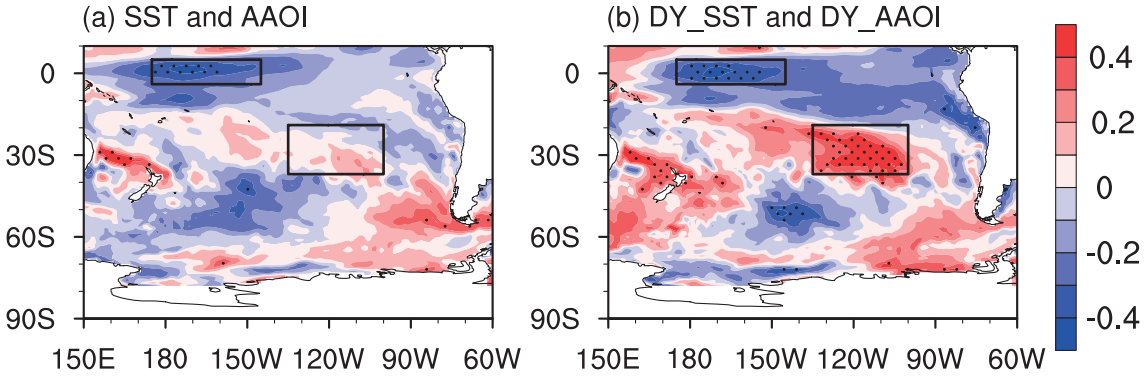

Fig. 7. (a) Correlation coefficients between the observed MAM AAOI and CFSv2-predicted SST during 1983–2015. (b) As in (a), but for the DY of SST and the DY of AAOI. Dotted areas indicate statistical significance at the 95% confidence level, based on the Student's *t*-test. The black curvilinear rectangles represent the key regions of SST influencing MAM AAO.

MAM DY_SSTI_R$_3$ (DY_SSTI_R$_4$), with a correlation coefficient of 0.53 (0.88) at the 99% confidence level, indicating a good performance of CFSv2 for the prediction of MAM DY_SSTI_R$_3$ (DY_SSTI_R$_4$). Accordingly, the CFSv2-predicted MAM DY_SSTI_R$_3$ and DY_SSTI_R$_4$ are used in the dynamical–statistical model for predicting MAM DY_AAOI.

4.2. *Dynamical–statistical model and results*

To improve the CFSv2-predicted MAM AAOI, a dynamical–statistical model is established to improve DY_AAOI utilizing the abovementioned predictors, i.e., DY_SICI_R$_1$, DY_SICI_R$_2$, DY_SSTI_R$_3$, and DY_SSTI_R$_4$. An improved CFSv2-predicted AAOI is expected to be obtained by adding the improved DY_AAOI prediction to the observed MAM AAOI for the previous year.

The dynamical–statistical model for MAM DY_AAOI prediction is established based on a multivariable regression method, as follows:

$$\mathrm{DY\_AAOI} = a(\mathrm{DY\_SICI\_R_1} - \mathrm{DY\_SICI\_R_2}) + b(\mathrm{DY\_SSTI\_R_3} - \mathrm{DY\_SSTI\_R_4}),$$

where DY_SICI_R$_1$ and DY_SICI_R$_2$ are the observed DY_SICI for the preceding SON for Region-1 and Region-2, respectively; DY_SSTI_R$_3$ and DY_SSTI_R$_4$ are the CFSv2-predicted DY_SSTI for the concurrent MAM for Region-3 and Region-4, respectively; a and b are the corresponding regression coefficients for the DY_SICI and DY_SSTI predictors, respectively.

The predictive skill of this dynamical–statistical model is evaluated using two-years-out validations (Michaelsen, 1987; Blockeel and Struyf, 2003). Figure 8a shows the cross-validation results of DY_AAOI prediction obtained from this dynamical–statistical model. It can be seen that the predicted MAM DY_AAOIs for the period 1983–2014 in the two-years-out cross-validation are largely consistent with the observed MAM DY_AAOI in terms of interannual variability, with correlation coefficients of 0.58 between the predicted and observed time series significant at the 99% confidence level. The RMSE between the dynamic–statistical model predicted and observed time series is 0.90, reduced by 34% relative to the RMSE between the time series of the CFSv2-predicted and observed DY_AAOI. In comparison to the insignificant correlation between the CFSv2-predicted and observed DY_AAOI, the dynamical–statistical model produces a notably improved DY_AAOI prediction.

Correspondingly, an improved AAOI prediction during

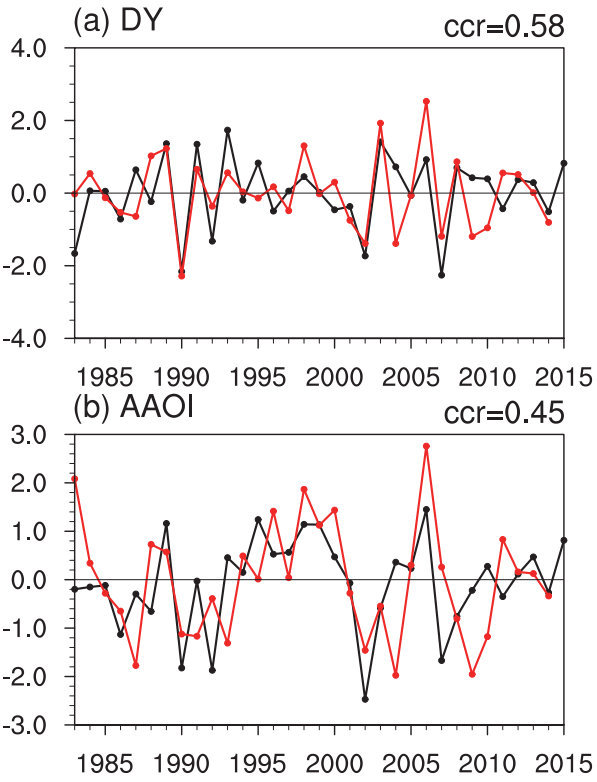

Fig. 8. Predicted and observed (a) DY of AAOI and (b) AAOI for 1983–2015, in which the predicted DY uses the dynamical–statistical prediction model in the cross-validations. The abbreviation ccr represents the correlation coefficient of the two indices between observation and prediction.

1983–2015 is obtained by adding the predicted MAM DY_AAOI in the cross-validations to the observed MAM AAOI for the previous year. The time series of this predicted MAM AAOI shows a general consistency with the time series of the observed MAM AAOI, with a correlation coefficient of 0.45 significant at the 99% confidence level (Fig. 8b). The RMSE between the dynamic–statistical model predicted and observed time series is 1.01, reduced by 25% relative to the RMSE between the time series of the CFSv2-predicted and observed MAM AAOI. On the other hand, there are several years where the predicted MAM AAOI still shows a discrepancy with the observed MAM AAOI, such as 1983, 1988, 1992, 1993, 2004, 2009, and 2010, in the cross-validation results (Fig. 8b), which are mainly due to the limitation of the DY_AAOI prediction (Fig. 8a). The interdecadal variability of the predicted MAM AAOI is essentially consistent with that of the observed MAM AAOI (Fig. 8b), exhibiting remarkable improvement relative to the CFSv2 prediction (Fig. 4a). Overall, the dynamical–statistical model demonstrates a considerable capability for improving the AAOI prediction of CFSv2.

5. Discussion

The predictive skill for MAM SIC and the atmospheric response to SIC in CFSv2 are further evaluated to find the possible reasons for the poor skill of predicting the AAO in CFSv2. Previous studies suggest that CFSv2 can capture the seasonal cycle, long-term trend and interannual variability of sea ice (Wang et al., 2013; Saha et al., 2014). Indeed, CFSv2 shows reasonable skill for MAM SIC/DY_SIC prediction over the Weddell Sea and Bellinsgauzen–Amundsen Sea (figure not shown). However, CFSv2 cannot predict the atmospheric response to sea ice (Fig. 9). Observationally, there is a significant AAO response to the MAM key sea ice, with significant negative (positive) values in high (mid) latitude regions (Figs. 9a and b). Unfortunately, there is no significant atmospheric response in the CFSv2 prediction, with insignificant signals appearing at high latitudes and few signals appearing at midlatitudes (Figs. 9c and d). This indicates a poor skill of CFSv2 for forecasting the atmospheric response to SIC. Hence, the unreliable predictive skill of CFSv2 in the response of the atmosphere to sea ice may be an important

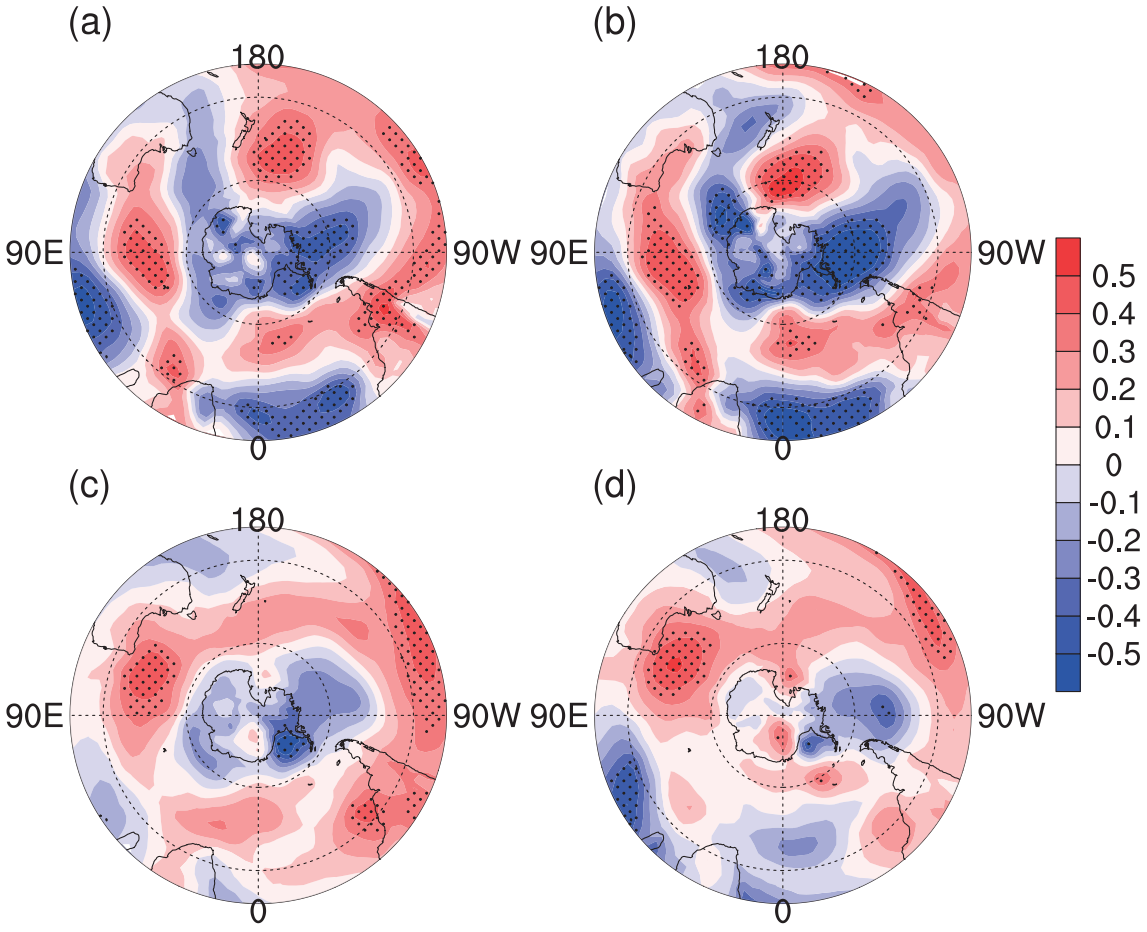

Fig. 9. (a) Correlation coefficients between the MAM SIC index and MAM SLP derived from observation during 1983–2015. (b) As in (a), but for the DY of sea ice and the DY of SLP. (c, d) As in (a, b), but for the CFSv2-predicted sea ice and SLP. The MAM SIC index is defined by the area-weighted areal mean of MAM SIC in the Weddell Sea (70°–75°S, 30°–55°W) minus the value in the Amundsen Sea (68°–75°S, 120°–150°W). Dotted areas indicate statistical significance at the 95% confidence level, based on the Student's *t*-test.

reason for the failure of CFSv2 to predict the AAO.

6. Conclusion

The capability of CFSv2 with respect to MAM AAO prediction is evaluated in this study. The CFSv2 prediction presents the spatial pattern of MAM SLP during 1983–2015 for the SH reasonably well, but underestimates the SLP over Antarctica. In addition, the interannual variability of MAM SLP for the period 1983–2015 is significantly underestimated in the CFSv2 prediction. Correspondingly, a poor performance of CFSv2 for MAM AAO prediction is found, where the CFSv2 prediction fails to present a zonally symmetric spatial pattern of the MAM AAO and the CFSv2-predicted AAOI has an insignificant correlation of 0.02 with the observed AAOI during 1983–2015. A dynamical–statistical model is established to improve the CFSv2 prediction for the AAOI, utilizing the interannual-increment approach and two predictors including the observed SIC for the preceding SON in the Weddell Sea and Bellinsgauzen–Amundsen Sea, and the CFSv2-predicted SST for the concurrent MAM over the midlatitude southeastern Pacific and equatorial central Pacific. The two-years-out cross-validation results indicate that the dynamical–statistical model can produce a much better prediction for DY_AAOI in comparison to the CFSv2 prediction, whereby a notably improved AAOI is obtained. Specifically, the correlation coefficient of the DY_AAOI between the observation and prediction in the dynamical–statistical model using the cross-validation (CFSv2 direct hindcast) is 0.58(0.03) during 1983–2015. After the improvement, the correlation coefficient of the AAOI increases from 0.02 to 0.45 during 1983–2015, which is significant at the 99% confidence level. Moreover, although CFSv2 can capture the climatological mean pattern and interannual variability of the MAM SIC to some extent, CFSv2 fails to simulate the response of the atmosphere to MAM sea ice, which may contribute to its failure in predicting the MAM AAO.

The good performance of this dynamical–statistical model demonstrates a capability of the interannual-increment approach for the interannual prediction of the MAM AAOI. The effect of the interannual-increment approach for amplifying signals of year-to-year variability applies to all variables and signals that have a considerable interannual variability, especially quasi-biennial oscillation. Hence, the interannual-increment approach may be used for improving the prediction of other factors, such as the Arctic Oscillation and East Asian summer monsoon, in the future.

During the past several decades, the AAO has exhibited a trend toward a positive phase (Marshall, 2007). This trend is expected to accelerate in the future because of an increase in greenhouse gases and a depletion of stratospheric ozone (Fyfe et al., 1999; Cai and Cowan, 2007; Hao et al., 2017). The impact of this trend of the AAO on the Northern Hemisphere climate warrants further study. In addition, the predictive skill of CFSv2 for the trend of the AAO needs examination.

Finally, it is important to acknowledge that this study focuses on the MAM AAO and does not examine the performance of CFSv2 for AAO prediction in other seasons. Predictors different from SIC and SST may be needed to establish a dynamical–statistical model for improving AAO prediction at other times of the year.

Acknowledgements. This work was supported by the National Key Research and Development Program of China (Grant No. 2016YFA0600703) and the funding of the Jiangsu Innovation & Entrepreneurship Team and the Priority Academic Program Development of Jiangsu Higher Education Institutions.

REFERENCES

Blockeel, H., and J. Struyf, 2003: Efficient algorithms for decision tree cross-validation. *Journal of Machine Learning Research*, **3**, 621–650.

Cai, W. J., and T. Cowan, 2007: Trends in southern hemisphere circulation in IPCC AR4 models over 1950–99: Ozone depletion versus greenhouse forcing. *J. Climate*, **20**, 681–693, https://doi.org/10.1175/JCLI4028.1.

Deser, C., R. A. Tomas, and S. L. Peng, 2007: The transient atmospheric circulation response to north atlantic SST and sea ice anomalies. *J. Climate*, **20**, 4751–4767, https://doi.org/10.1175/JCLI4278.1.

Fan, K., 2009a: Linkage between the atlantic tropical hurricane frequency and the antarctic oscillation in the western hemisphere. *Atmospheric and Oceanic Science Letters*, **2**, 159–164, https://doi.org/10.1080/16742834.2009.11446796.

Fan, K., 2009b: Predicting winter surface air temperature in Northeast China. *Atmospheric and Oceanic Science Letters*, **2**, 14–17, https://doi.org/10.1080/16742834.2009.11446770.

Fan, K., 2009c: Seasonal forecast model for the number of tropical cyclones to make landfall in China. *Atmospheric and Oceanic Science Letters*, **2**, 251–254, https://doi.org/10.1080/16742834.2009.11446811.

Fan, K., and H. J. Wang, 2004: Antarctic oscillation and the dust weather frequency in North China. *Geophys. Res. Lett.*, **31**, L10201, https://doi.org/10.1029/2004GL019465.

Fan, K., and H. J. Wang, 2006: Interannual variability of Antarctic Oscillation and its influence on East Asian climate during boreal winter and spring. *Science in China Series D*, **49**, 554–560, https://doi.org/10.1007/s11430-006-0554-7.

Fan, K., and H. J. Wang, 2007: Simulation of the AAO anomaly and its influence on the Northern Hemispheric circulation in boreal winter and spring. *Chinese Journal of Geophysics*, **50**, 397–403, https://doi.org/10.3321/j.issn:0001-5733.2007.02.009. (in Chinese with English abstract)

Fan, K., and H. Liu, 2013: Evaluation of atmospheric circulation in the southern hemisphere in 20CRv2. *Atmospheric and Oceanic Science Letters*, **6**, 337–342.

Fan, K., B. Q. Tian, and H. J. Wang, 2016: New approaches for the skillful prediction of the winter North Atlantic Oscillation based on coupled dynamic climate models. *International Journal of Climatology*, **36**, 82–94, https://doi.org/10.1002/joc.4330.

Fan, K., H. J. Wang, and Y. J. Choi, 2008: A physically-based statistical forecast model for the middle-lower reaches of the Yangtze River Valley summer rainfall. *Chinese Science Bul-*

letin, **53**, 602–609, https://doi.org/10.1007/s11434-008-0083-1.

Fyfe, J. C., G. J. Boer, and G. M. Flato, 1999: The Arctic and Antarctic Oscillations and their projected changes under global warming. *Geophys. Res. Lett.*, **26**, 1601–1604, https://doi.org/10.1029/1999GL900317.

Gao, H., F. Xue, and H. J. Wang, 2003: Influence of interannual variability of Antarctic Oscillation on Mei-yu along the Yangtze and Huaihe River valley and its importance to prediction. *Chinese Science Bulletin*, **48**, 61–67.

Gong, D. Y., and S. W. Wang, 1998: Antarctic Oscillation: Concept and applications. *Chinese Science Bulletin*, **43**, 734–738, https://doi.org/10.1007/BF02898949.

Gong, D. Y., and S. W. Wang, 1999: Definition of Antarctic Oscillation index. *Geophys. Res. Lett.*, **26**, 459–462, https://doi.org/10.1029/1999GL900003.

Gupta, A. S., and M. H. England, 2007: Coupled ocean–atmosphere feedback in the southern annular mode. *J. Climate*, **20**, 3677–3692, https://doi.org/10.1175/JCLI4200.1.

Han, T. T., H. J. Wang, and J. Q. Sun, 2017: Strengthened relationship between the antarctic oscillation and enso after the mid-1990s during austral spring. *Adv. Atmos. Sci.*, **34**, 54–65, https://doi.org/10.1007/s00376-016-6143-6.

Hao, X., S. P. He, H. J. Wang, and T. T. Han, 2017: The impact of long-term oceanic warming on the antarctic oscillation in austral winter. *Scientific Reports*, **7**, 12321, https://doi.org/10.1038/s41598-017-12517-x.

Hendon, H. H., D. W. J. Thompson, and M. C. Wheeler, 2007: Australian rainfall and surface temperature variations associated with the Southern Hemisphere annular Mode. *J. Climate*, **20**, 2452–2467, https://doi.org/10.1175/JCLI4134.1.

Huang, Y. Y., H. J. Wang, and K. Fan, 2014: Improving the prediction of the summer Asian-Pacific Oscillation using the interannual increment approach. *J. Climate*, **27**, 8126–8134, https://doi.org/10.1175/JCLI-D-14-00209.1.

Jiang, X. W., S. Yang, Y. Q. Li, A. Kumar, W. Q. Wang, and Z. T. Gao, 2013: Dynamical prediction of the east asian winter monsoon by the ncep climate forecast system. *J. Geophys. Res.*, **118**, 1312–1328, https://doi.org/10.1002/jgrd.50193.

Kalnay E., and Coauthors, 1996: The NCEP/NCAR 40-year reanalysis project. *Bull. Amer. Meteor. Soc.*, **77**, 437–472, https://doi.org/10.1175/1520-0477(1996)077<0437:TNYRP>2.0.CO;2.

Kumar, A., M. Chen, L. Zhang, W. Wang, Y. Xue, C. Wen, L. Marx, and B. Huang, 2012: An analysis of the nonstationarity in the bias of sea surface temperature forecasts for the NCEP Climate Forecast System (CFS) version 2. *Mon. Wea. Rev.*, **140**, 3003–3016, https://doi.org/10.1175/MWR-D-11-00335.1.

Kushnir, Y., W. A. Robinson, I. Bladé, N. M. J. Hall, S. Peng, and R. Sutton, 2002: Atmospheric GCM response to extratropical SST anomalies: Synthesis and evaluation. *J. Climate*, **15**, 2233–2256, https://doi.org/10.1175/1520-0442(2002)015<2233:AGRTES>2.0.CO;2.

Li, F., H. J. Wang, and Y. Q. Gao, 2015: Modulation of Aleutian Low and Antarctic oscillation co-variability by ENSO. *Climate Dyn.*, **44**, 1245–1256, https://doi.org/10.1007/s00382-014-2134-4.

Lim, E. P., H. H. Hendon, and H. Rashid, 2013: Seasonal predictability of the Southern Annular mode due to its association with ENSO. *J. Climate*, **26**, 8037–8054, https://doi.org/10.1175/JCLI-D-13-00006.1.

Limpasuvan, V., and D. L. Hartmann, 2000: Wave-maintained annular modes of climate variability. *J. Climate*, **13**, 4414–4429, https://doi.org/10.1175/1520-0442(2000)013<4414:WMAMOC>2.0.CO;2.

Lovenduski, N. S., and N. Gruber, 2005: Impact of the Southern Annular mode on Southern Ocean circulation and biology. *Geophys. Res. Lett.*, **32**, L11603, https://doi.org/10.1029/2005GL022727.

Marshall, G. J., 2007: Half-century seasonal relationships between the Southern Annular mode and Antarctic temperatures. *International Journal of Climatology*, **27**, 373–383, https://doi.org/10.1002/joc.1407.

Marshall, G. J., and T. J. Bracegirdle, 2015: An examination of the relationship between the Southern Annular Mode and Antarctic surface air temperatures in the CMIP5 historical runs. *Climate Dyn.*, **45**, 1513–1535, https://doi.org/10.1007/s00382-014-2406-z.

Michaelsen, J., 1987: Cross-validation in statistical climate forecast models. *J. Climate Appl. Meteor.*, **26**, 1589–1600, https://doi.org/10.1175/1520-0450(1987)026<1589:CVISCF>2.0.CO;2.

Mo, K. C., 2000: Relationships between low-frequency variability in the Southern Hemisphere and sea surface temperature anomalies. *J. Climate*, **13**, 3599–3610, https://doi.org/10.1175/1520-0442(2000)013<3599:RBLFVI>2.0.CO;2.

Pokhrel, S., H. Rahaman, A. Parekh, S. K. Saha, A. Dhakate, H. S. Chaudhari, and R. M. Gairola, 2012: Evaporation-precipitation variability over Indian Ocean and its assessment in NCEP Climate Forecast System (CFSv2). *Climate Dyn.*, **39**, 2585–2608, https://doi.org/10.1007/s00382-012-1542-6.

Raphael, M. N., W. Hobbs, and I. Wainer, 2011: The effect of Antarctic sea ice on the Southern Hemisphere atmosphere during the southern summer. *Climate Dyn.*, **36**, 1403–1417, https://doi.org/10.1007/s00382-010-0892-1.

Rayner, N. A., D. E. Parker, E. B. Horton, C. K. Folland, L. V. Alexander, D. P. Rowell, E. C. Kent, and A. Kaplan, 2003: Global analyses of sea surface temperature, sea ice, and night marine air temperature since the late nineteenth century. *J. Geophys. Res.*, **108**, 4407, https://doi.org/10.1029/2002JD002670.

Riddle, E. E., A. H Butler., J. C. Furtado, J. L. Cohen, and A. Kumar, 2013: CFSv2 ensemble prediction of the wintertime Arctic Oscillation. *Climate Dyn.*, **41**, 1099–1116, https://doi.org/10.1007/s00382-013-1850-5.

Saha S., and Coauthors, 2014: The NCEP climate forecast system version 2. *J. Climate*, **27**, 2185–2208, https://doi.org/10.1175/JCLI-D-12-00823.1.

Screen, J. A., N. P. Gillett, A. Y. Karpechko, and D. P. Stevens, 2010: Mixed layer temperature response to the southern annular mode: Mechanisms and model representation. *J. Climate*, **23**, 664–678, https://doi.org/10.1175/2009JCLI2976.1.

Seager, R., N. Harnik, and Y. Kushnir, 2003: Mechanisms of hemispherically symmetric climate variability. *J. Climate*, **16**, 2960–2978, https://doi.org/10.1175/1520-0442(2003)016<2960:MOHSCV>2.0.CO;2.

Silvestri, G. E., and C. S. Vera, 2003: Antarctic Oscillation signal on precipitation anomalies over southeastern South America. *Geophys. Res. Lett.*, **30**, 2115, https://doi.org/10.1029/2003GL018277.

Smith, T. M., R. W. Reynolds, T. C. Peterson, and J. Lawrimore, 2008: Improvements to NOAA's historical merged land–ocean surface temperature analysis (1880–2006). *J. Climate*,

21, 2283–2296, https://doi.org/10.1175/2007JCLI2100.1.

Stammerjohn, S. E., and R. C. Smith, 1997: Opposing Southern Ocean climate patterns as revealed by trends in regional sea ice coverage. *Climatic Change*, **37**, 617–639, https://doi.org/10.1023/A:1005331731034.

Stammerjohn, S. E., D. G. Martinson, R. C. Smith, X. J. Yuan, and D. Rind, 2008: Trends in Antarctic annual sea ice retreat and advance and their relation to El Niño-Southern Oscillation and Southern Annular mode variability. *J. Geophys. Res.*, **113**, C03S90, https://doi.org/10.1029/2007JC004269.

Sun, B., and H. J. Wang, 2013: Larger variability, better predictability? *International Journal of Climatology*, **33**, 2341–2351, https://doi.org/10.1002/joc.3582.

Sun, J. Q., 2010: Possible impact of the boreal spring Antarctic oscillation on the North American summer monsoon. *Atmospheric and Oceanic Science Letters*, **3**, 232–236, https://doi.org/10.1080/16742834.2010.11446870.

Sun, J. Q., H. J. Wang, and Y. Wei, 2009: A possible mechanism for the co-variability of the boreal spring Antarctic Oscillation and the Yangtze River valley summer rainfall. *International Journal of Climatology*, **29**, 1276–1284, https://doi.org/10.1002/joc.1773.

Thompson, D. W. J., and J. M. Wallace, 2000: Annular modes in the extratropical circulation. Part I: Month-to-month variability. *J. Climate*, **13**, 1000–1016, https://doi.org/10.1175/1520-0442(2000)013<1000:AMITEC>2.0.CO;2.

Thompson, D. W. J., and S. Solomon, 2002: Interpretation of recent Southern Hemisphere climate change. *Science*, **296**, 895–899, https://doi.org/10.1126/science.1069270.

Tian, B. Q., and K. Fan, 2015: A skillful prediction model for winter NAO Based on Atlantic sea surface temperature and Eurasian snow cover. *Wea. Forecasting*, **30**, 197–205, https://doi.org/10.1175/WAF-D-14-00100.1.

Tian, B. Q., K. Fan, and H. Q. Yang, 2018: East Asian winter monsoon forecasting schemes based on the NCEP's climate forecast system. *Climate Dyn.*, **51**, 2793–2805, https://doi.org/10.1007/s00382-017-4045-7.

Wang, H. J., Y. Zhang, and X. M. Lang, 2010: On the predictand of short-term climate prediction. *Climatic and Environmental Research*, **15**, 225–228. (in Chinese with English abstract)

Wang, W. Q., M. Y. Chen, and A. Kumar, 2013: Seasonal prediction of Arctic sea ice extent from a coupled dynamical forecast system. *Mon. Wea. Rev.*, **141**, 1375–1394, https://doi.org/10.1175/MWR-D-12-00057.1.

Wu, Q. G., and X. D. Zhang, 2011: Observed evidence of an impact of the Antarctic sea ice dipole on the Antarctic Oscillation. *J. Climate*, **24**, 4508–4518, https://doi.org/10.1175/2011JCLI3965.1.

Xu, X. P., F. Li, S. P. He, and H. J. Wang, 2018: Subseasonal reversal of East Asian surface temperature variability in winter 2014/15. *Adv. Atmos. Sci.*, **35**, 737–752, https://doi.org/10.1007/s00376-017-7059-5.

Xue, F., H. J. Wang, and J. H. He, 2003: Interannual variability of Mascarene high and Australian high and their influences on summer rainfall over East Asia. *Chin. Sci. Bull.*, **48**, 492–497, https://doi.org/10.1007/BF03183258.

Yin, Z. C., and H. J. Wang, 2016: Seasonal prediction of winter haze days in the north central north china plain. *Atmos. Chem. Phys.*, **16**, 14 843–14 852, https://doi.org/10.5194/acp-16-14843-2016.

Zhang, J. L., 2007: Increasing Antarctic sea ice under warming atmospheric and oceanic conditions. *J. Climate*, **20**, 2515–2529, https://doi.org/10.1175/JCLI4136.1.

Zhou, T. J., and R. C. Yu, 2004: Sea-surface temperature induced variability of the Southern Annular Mode in an atmospheric general circulation model. *Geophys. Res. Lett.*, **31**, L24206, https://doi.org/10.1029/2004GL021473.